Helsinki University of Technology
Laboratory of Applied Thermodynamics/CFD-Group

MEMO No CFD/TERMO-22-97 DATE: November 21, 1997

TITLE

GRV-60 Impeller with airfoil-type and unvaned diffusor

AUTHOR(S)
Harri Heiska

ABSTRACT

Reynolds averaged Navier-Stokes (RANS) calculations are performed for the GRV-60 radial impeller with an airfoil-type and an unvaned diffusor. For the the airfoil-type aerodynamic diffusor design and off-design conditions are investigated at $N = 14000$ RPM. Design conditions are investigated at $N = 16000$ RPM. For the unvaned diffusor design conditions are studied at $N = 16000$ RPM. Measured total pressure ratios $\pi_{tot,16}$ and isentropic efficiency values $\eta_{i,16}$ in [4] are compared with the calculated values. The results are in good agreement with measurements.

MAIN RESULT

PAGES
18

KEY WORDS
FINFLO, Impeller, high-speed technology

APPROVED BY

Timo Siikonen November 21, 1997

1 Nomenclature

A	area
CFL	Courant number
D	diameter
E	total internal energy per unit volume
H	total enthalpy
Ma	Mach number
N	shaft speed
P	power
P_S	isentropic power
R	gas constant
Re	Reynolds number
T	temperature, also torque
U	vector of the conservative variables
$\vec{V}$	velocity
c_p	specific heat at constant pressure
c_v	specific heat at constant volume
e	specific internal energy
h	enthalpy
$\dot{m}$	mass flow rate
p	static pressure
r	radius
y^+	cell height - a nondimensional normal distance from the surface
α,β,γ,δ,ϵ	coefficients
γ	ratio of specific heats $\gamma = c_p/c_v$
η	efficiency
λ	nondimensional radius
ρ	density
ω	angular velocity
π	pressure ratio
u, v, w	velocity compenents in x-, y- and z-direction
x, y, z	Cartesian coordinates

Subscripts

cfd	calculation result
i,16	isentropic value at $\lambda = 1.6$
ref	reference condition or measured value
tot,16	value based on total conditions at $\lambda = 1.6$
0	total (stagnation) value

Superscripts

$+$	nondimensional value

2 Acknowledgements

This study is made in co-operation and by the order of the High Speed Technology research group of Lappeenranta University of Technology (LUT). The geometry and measured values of GRV-60 radial compressor is given by the laboratory of Professor Manfred Rautenberg, Hannover University, to the High Speed Technology research group of LUT.

3 About Finflo

Finflo is a general purpose 3D Reynolds averaged Navier-Stokes solver for compressible and incompressible flows with non-rotating and rotating geometries. Roe's flux-difference splitting is used for the solution of Reynolds-averaged Navier-Stokes equations. Turbulence is modelled with low-Reynolds number turbulence models. Currently algebraic, $k-\epsilon$, and Reynolds stress models are implemented in the code. No universal wall-functions are applied in the turbulence modelling. In the present calculations turbulence is modelled using Baldwin-Lomax algebraic turbulence model. A multigrid algorithm is used to accelerate the convergence. The main features of the solution method are described in [1] and [2].

Investigated geometries are discreticed with structured control volume meshes using the IGG grid generator [3]. Complex geometries are divied into multiple grid blocks. In constructing the grid, a block face or a part of if is connected to a corresponding part of an another block face. Currently these parts must be identical. If one grid block is rotating and another is non-rotating, then the face must be on a rotational surface. In this way a block can also be given with a fixed angle of rotation in connection with another block. In these calculations this angle is $\theta = 0$ radians. In the current version of Finflo axis of rotation is the x-axis.

4 Impeller and Stator Geometry

GRV-60 impeller has 20 channels. Every second blade is cut. Rotor blade leading and trailing edges are rounded. In the modelled part of the impeller there are two channels with a full blade and with another cut blade. Tip clearance is not modelled between the blade tip and the shroud surface. The airfoil-type diffusor is modelled using one blade with rounded leading and trailing edges and constant height between $r = 0.2 \ldots 0.4$ m. In the modelled geometry the diffusor channel is connected with two impeller channels. In the actual aerodynamic diffusor there are 21 channels. The unvaned diffusor is modelled with constant area between $r = 0.2 \ldots 0.4$ m. The first cell height is $8 \cdot 10^{-6}$ m, which corresponds to $y^+ = 2 \ldots 3$. It should be pointed out that the trailing edge of the impeller blade is different from the actual geometry where it is blunt instead of being rounded. At the trailing edge of the blade the shroud radius is larger than the hub radius. In the actual geometry the radius is constant at the blade trailing edge. In the following equations, figures and results a nondimensional radius λ is used to indicate radial distance from the rotational axis. It is defined as $\lambda = r/r_{0.2}$. The following figures (1), (2), (3) and (4) show the modelled surface grid geometry and the meridional projection view for both cases. The surface mesh is shown in the Fig. (3). A two-dimensional meridional projection view of the impeller with the unvaned diffusor is shown in Fig. (4). A two-dimensional meridional projection view of the impeller with the unvaned diffusor is shown in Fig. (2). The grid dimensions for the impeller with the airfoil-type diffusor are

BLOCK	IMAX	JMAX	KMAX	CELLS
1	64	48	128	393 216
2	64	48	128	393 216
3	128	48	48	294 912
4	128	48	128	786 432
TOTAL NUMBER OF CELLS				1 867 776

The grid dimensions for the impeller with the unvaned diffusor are

BLOCK	IMAX	JMAX	KMAX	CELLS
1	64	48	128	393 216
2	64	48	128	393 216
3	128	48	48	294 912
4	128	48	96	589 824
TOTAL NUMBER OF CELLS				1 671 168

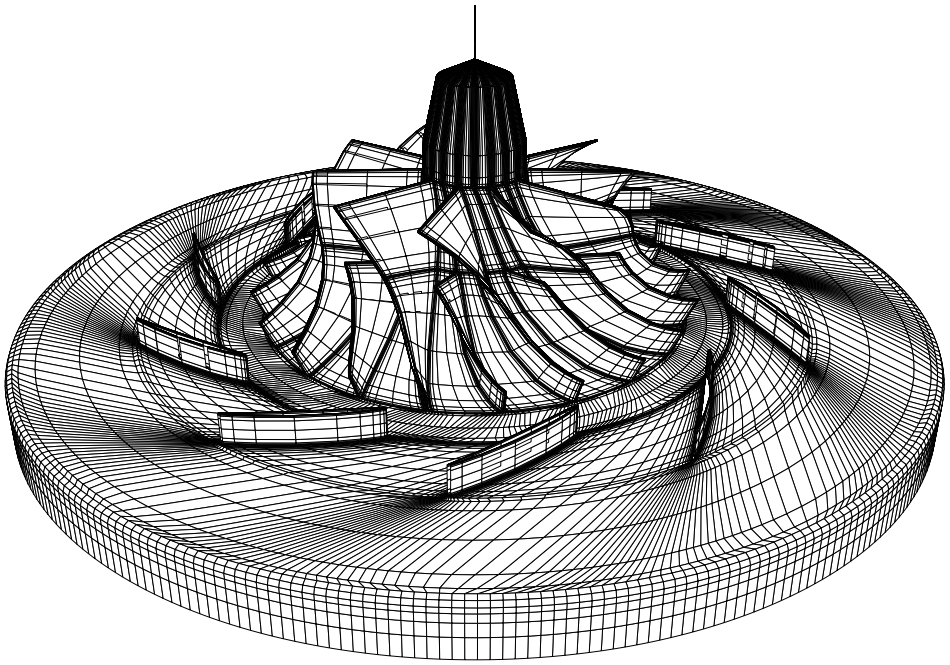

Fig. 1: Impeller with an airfoil-type diffusor. The grid is shown on the 3rd level.

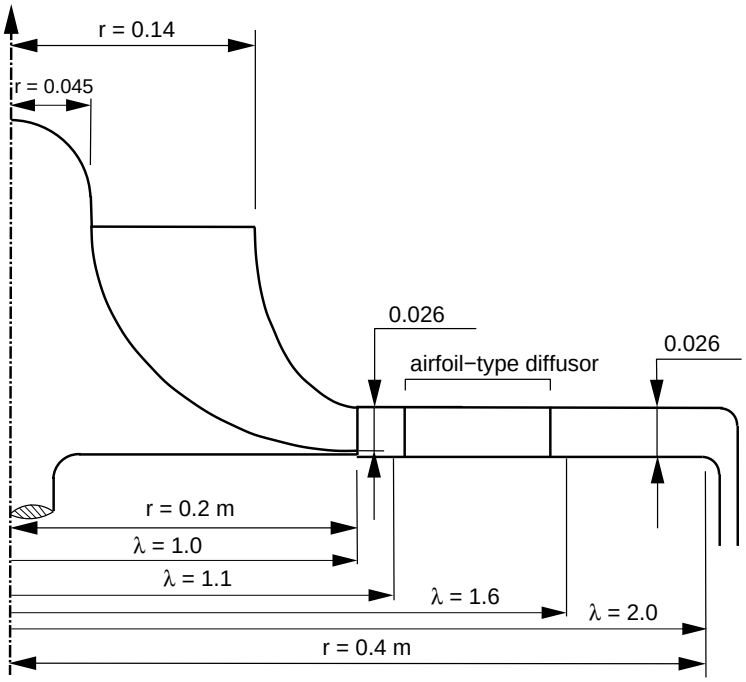

Fig. 2: Meridional projection view of the impeller with the airfoil-type diffusor.

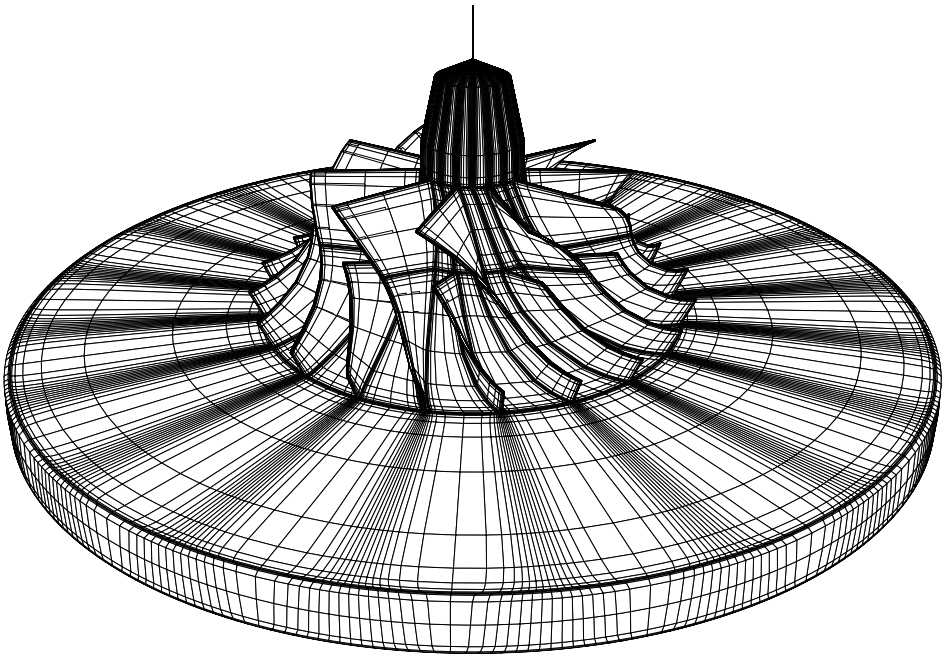

Fig. 3: Impeller with the unvaned diffusor. Grid is shown on the 3rd level.

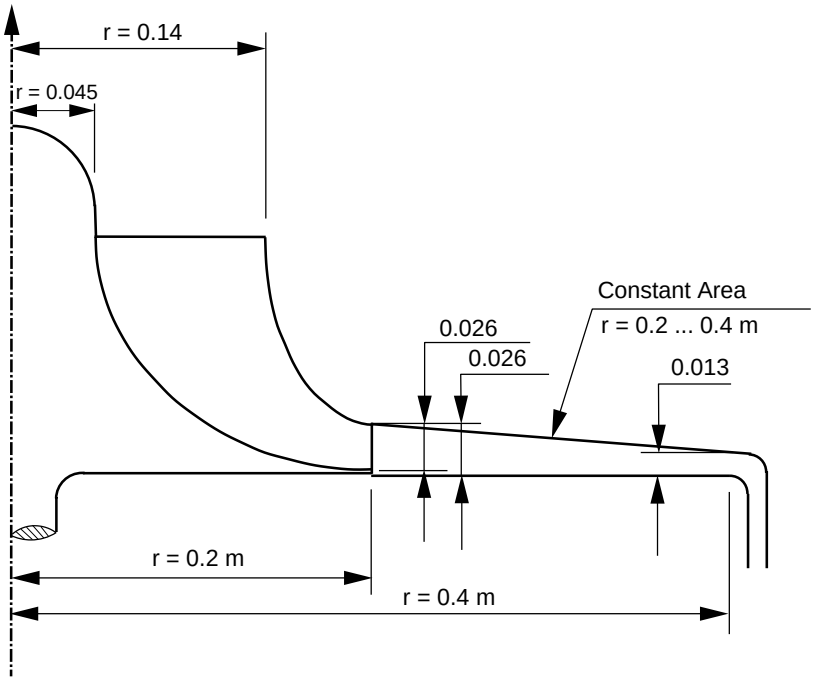

Fig. 4: Meridional projection view of the impeller with the unvaned diffusor.

5 Test cases

The cases listed in Tables (1) and (2) were selected to be calculated with Finflo. The impeller with the airfoil-type diffusor was calculated with $N = 14000$ RPM and $N = 16000$ RPM. The impeller with the unvaned diffusor was calculated with $N = 16000$ RPM.

5.1 Initial values and boundary conditions

Initial values for the test cases were calculated with a one dimensional flow assumptions and these values were used as a starting point for the Finflo calculations. Used boundary conditions at the inlet are saved in DIST-files. The saved boudary values at each cell center are $U = (\rho, \rho u, \rho v, \rho w, E)^T$. The actual boundary value calculation method is chosen via INPUT-file. In these calculations at inlet the boundary value type is 2 and at outlet it is 2. At the inlet this means that $\dot{m}$ and H are specified as well as the flow angle, whereas density is extrapolated from the flowfield. At the outlet p is held constant. Because the actual measured static pressure before the collection chamber is not known, it is guessed. For this reason several outlet static pressure values had to be calculated for each test case. Used initial values are collected in Tables (1) and (2). In principle the pressure

N	$\dot{m}_{red}$	T_{01}	p_{01}	$\pi_{tot,16}$	$\eta_{i,16}$
RPM	$[kg/s]$	$[K]$	$[Pa]$	$[-]$	$[-]$
14000	4.65	288.15	101325	1.83	0.87
14000	6.26	288.15	101325	1.60	0.76
16000	5.74	288.15	101325	2.17	0.89

Table. 1: Boundary conditions and the measured values for the GRV-60 impeller with the airfoil-type diffusor.

N	$\dot{m}_{red}$	T_K	p_K	$\pi_{tot,16}$	$\eta_{i,16}$
RPM	$[kg/s]$	$[K]$	$[Pa]$	$[-]$	$[-]$
16000	5.51	288.15	101325	2.18	0.89

Table. 2: Boundary conditions and the measured values for the GRV-60 impeller with the unvaned diffusor.

before the impeller is obtained from the known total pressure and temperature. Since the code extrapolates one thermodynamic quantity from the flowfield, the calculated state at the inlet depends on the specified outlet pressure. The values of p_{01} and T_{01} are given in the collection chamber before the impeller. These values are converted for each flow case. After the conversion the DIST-files containing boundary value distributions are generated with a NEWBOUND -program. The following tables contain initial values for each flow case. Tube area for the radius $r = 0.14$ m is $A = 0.061575\ m^2$. The velocity distribution is assumed to be uniform and in the direction of the rotation axis since no velocity distributions are available.

The specific heat is $c_p = 1004.5\ J/(kgK)$. The total enthalpy is calculated from $H = c_p T_0$. The static pressure at the outlet p_{out} is guessed from the pressure ratio $\pi_{tot,16}$, since there is no measured value for the outlet static pressure. However, the static pressure can be estimated from the known total pressure ratio. At least two different values for p_{out} were calculated for each case in order to get the 2nd level result close enough for the given p_{in}. Only the 2nd level results are displayed, since in practice 3rd level grid is too coarse to give accurate enough computational results and 1st level calculations are not currently practical due to memory requirements and long calculation time.

N	$\dot{m}_{red}$	p_{01}	T_{01}	$\vec{V}$	H	p_{out}
RPM	$[kg/s]$	$[Pa]$	$[K]$	$[m/s]$	[J/g]	[kPa]
14000	4.65	97534	290.25	66.21	293744	160, 200
14000	6.26	99620	291.05	85.25	287193	140, 150, 160
16000	5.74	97856	291.05	76.09	289447	150, 160

Table. 3: Boundary values for the GRV-60 impeller with the airfoil-type diffusor.

N	$\dot{m}_{red}$	p_{01}	T_{01}	$\vec{V}$	H	p_{out}
RPM	$[kg/s]$	$[Pa]$	$[K]$	$[m/s]$	[J/g]	[kPa]
16000	5.51	96000	291.05	70.95	292360	160, 170

Table. 4: Boundary values for the GRV-60 impeller with the unvaned diffusor.

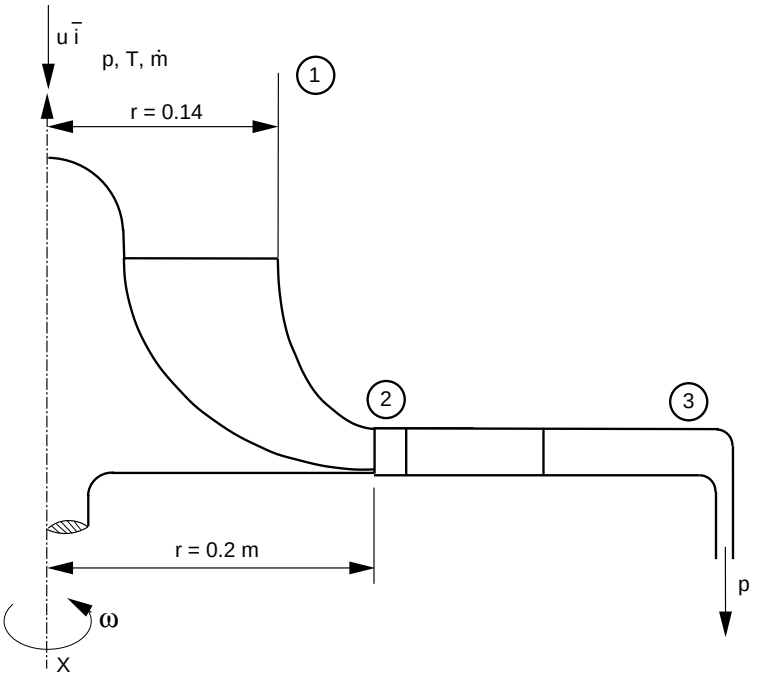

Fig. 5: Locations used in calculations.

6 Results

For a given case calculations are considered to be converged after the mass flow rate $\dot{m}$ does not differ too much from the given value. Level 2 results are considered to be reliable enough to be used for efficiency estimation. At least 2000 iteration cycles are needed for the 2nd level result to be converged. The calculated results are scaled to match the measured values. Scaling equations are

$$\dot{m}_{ref} = \dot{m}_{cfd} \frac{p_{01_{ref}}}{p_{01_{cfd}}} \sqrt{\frac{T_{01_{cfd}}}{T_{01_{ref}}}} \tag{1}$$

$$N_{ref} = N_{cfd} \sqrt{\frac{T_{01_{ref}}}{T_{01_{cfd}}}} \tag{2}$$

The isentropic efficiency $\eta_{i,16}$ is calculated using total values [5]

$$\eta_{i,16} = \frac{(p_{03}/p_{01})^{\frac{\gamma-1}{\gamma}} - 1}{(T_{03}/T_{01}) - 1} \tag{3}$$

The total values p_0 and T_0 are calculated using the local averaged Ma with the following equations

$$p_0/p = \left(1 + \frac{\gamma-1}{2} Ma^2\right)^{\frac{\gamma}{\gamma-1}} \tag{4}$$

$$T_0/T = 1 + \frac{\gamma-1}{2} Ma^2 \tag{5}$$

The static temperature is calculated from the massflow-averaged enthalpy h using the equation

$$c_p = R \cdot (\alpha + \beta T + \gamma T^2 + \delta T^3 + \epsilon T^4) \tag{6}$$

where for the ideal gas air the coefficients are: $\alpha = 3.653$, $\beta = -1.337 \cdot 10^{-3}$, $\gamma = 3.294 \cdot 10^{-6}$, $\delta = -1.913 \cdot 10^{-9}$ and $\epsilon = 0.2763 \cdot 10^{-12}$ [6]. The temperature is calculated from the equation $h = \int_{T_1}^{T_2} c_p(T) dt$. The isentropic efficiency η_S based on the calculated power for the impeller is calculated from

$$\eta_S = \frac{P_S}{P} = \frac{\dot{m} c_p \left[(p_{03}/p_{01})^{R/c_p} - 1\right] T_{01}}{\omega T} \tag{7}$$

where ωT is read from the FORCES file and p_{03} and p_{01} are read from the MCHECK file. In the following the isentropic efficiency calculated in this way is the most accurate one and is used in the comparison with the experimental data. The places where the value is averaged are shown in figure 5. Tables 5 and 6 contain the calculations results which have been scaled to match the measured values. Slightly different N_{ref} and $\dot{m_{ref}}$ are results from different p_{out} values. The values in tables 5 and 6 have been plotted in figures 6, 8, 7, and 9, and have been compared with measurements.

N_{ref}	$\dot{m_{ref}}$	$\eta_{S_{ref}}$	$\eta_{S_{cfd}}$	$\eta_{i,16_{cfd}}$	$\eta_{i,20_{cfd}}$	$\pi_{tot,16_{ref}}$	$\pi_{tot,16_{cfd}}$	$\pi_{tot,20_{cfd}}$	p_{out}
RPM	$[kg/s]$	$[-]$	$[-]$	$[-]$	[-]	$[-]$	[-]	[-]	[kPa]
13863	3.709	0.87	0.763	0.660	0.671	1.83	1.824	1.766	200
13840	4.832	0.87	0.822	0.663	0.831	1.83	1.797	1.732	160
13952	6.571	0.76	0.800	0.647	0.825	1.60	1.728	1.659	140
15802	6.723	0.89	0.851	0.664	0.842	2.17	2.080	2.014	160
15850	7.400	0.89	0.850	0.660	0.852	2.17	2.059	1.997	150

Table. 5: Initial values and calculation results for the GRV-60 impeller with the airfoil-type diffusor.

N_{ref}	$\dot{m}_{ref}$	$\eta_{i,16_{ref}}$	$\eta_{S_{cfd}}$	$\eta_{i,16_{cfd}}$	$\eta_{i,20_{cfd}}$	$\pi_{tot,16_{ref}}$	$\pi_{tot,16_{cfd}}$	$\pi_{tot,20_{cfd}}$	p_{out}
RPM	$[kg/s]$	$[-]$	$[-]$	$[-]$	[-]	$[-]$	[-]	[-]	[kPa]
15819	6.125	0.89	0.890	0.625	0.821	2.18	2.217	2.143	170
15799	6.704	0.89	0.888	0.624	0.818	2.18	2.177	2.110	160

Table. 6: Initial values and calculation results for the GRV-60 impeller with the unvaned diffusor.

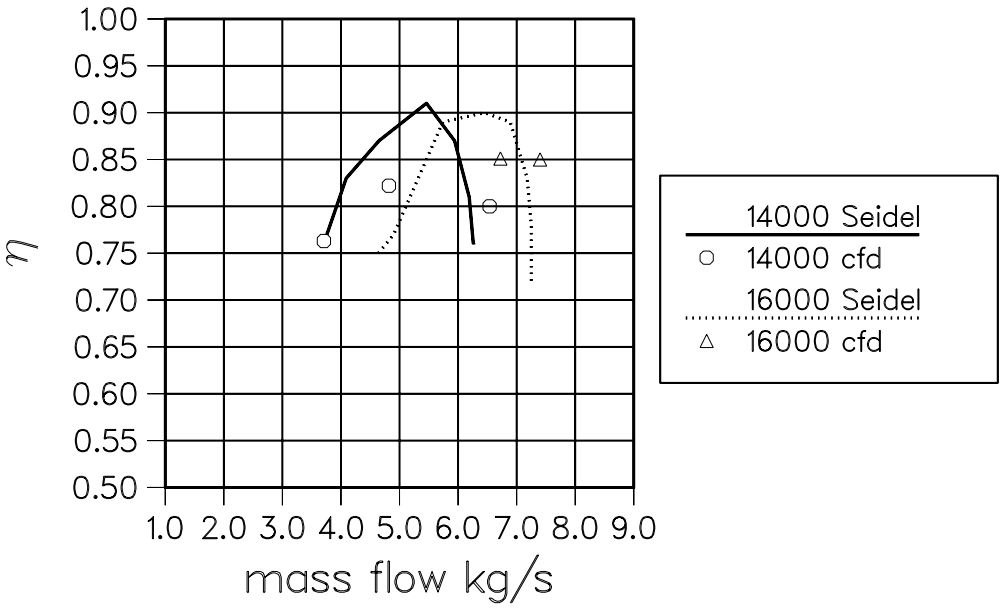

Fig. 6: Comparison of calculated η_S and measured $\eta_{i,16}$ for the GRV-60 impeller with the airfoil-type diffusor.

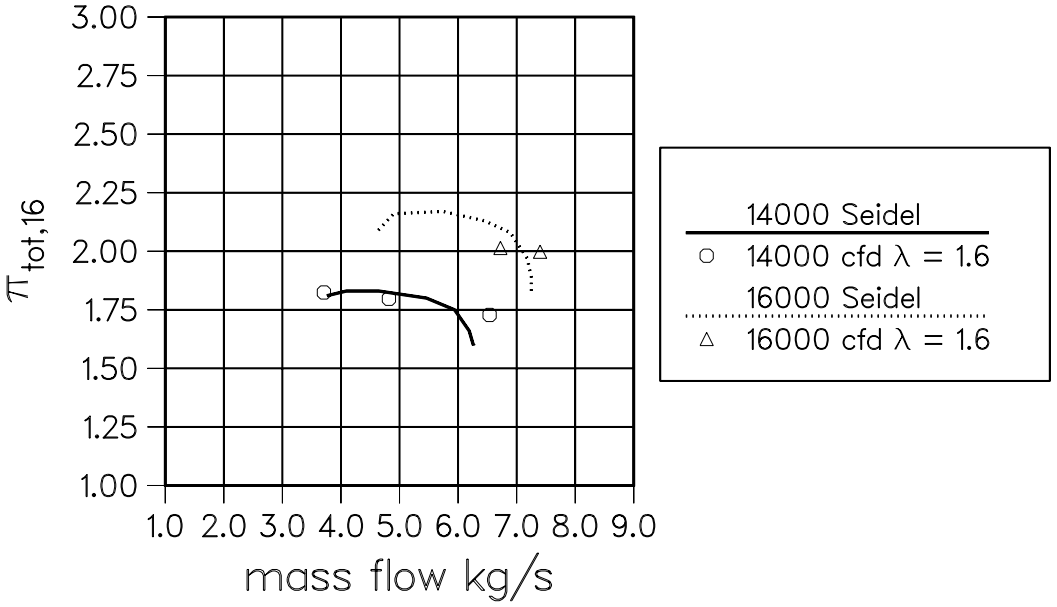

Fig. 7: Comparison of calculated $\pi_{tot,16}$ and measured $\pi_{tot,16}$ for the GRV-60 impeller with the airfoil-type diffusor.

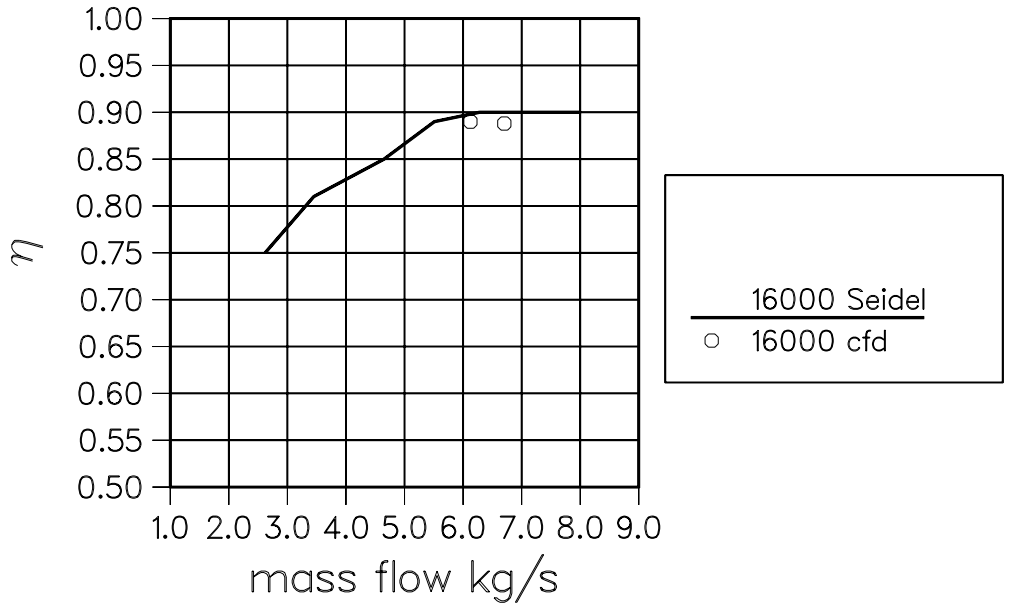

Fig. 8: Comparison of calculated η_S and measured $\eta_{i,16}$ for the GRV-60 impeller with the unvaned diffusor.

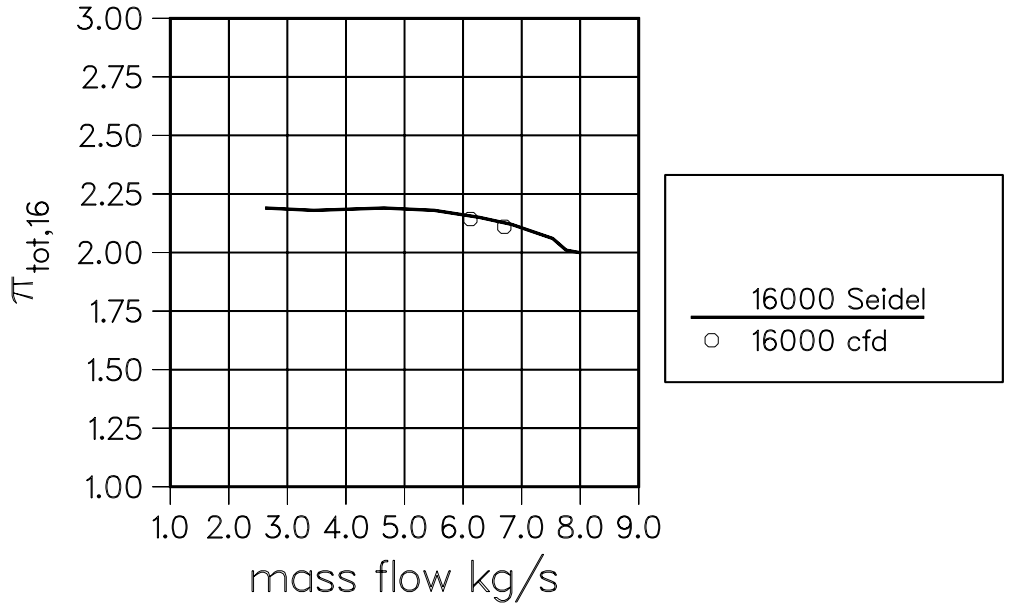

Fig. 9: Comparison of calculated $\pi_{tot,16}$ and measured $\pi_{tot,16}$ for the GRV-60 impeller with the unvaned diffusor.

7 Conclusions

Efficiencies and pressure ratios have been calculated from computational results for GRV-60 radial impeller with two different diffusors. The results show that the efficiencies and the pressure ratios can be calculated from the computational results with a good accuracy if the initial state is known before and the computational geometry is modelled with a sufficient accuracy. The efficiency is most accurately calculated from the calculated shaft power ωT. This is because of problem in the averaging of a total temperature. Consequently, the efficiency defined in this way is utilized in the comparisons with the experiments. If the calculation of boundary conditions is changed from the one used in this work, it should be possible to fix the inlet conditions and let the outlet conditions be defined according to the computational result. It should be pointed out that in order to expand the operational envelope of the computational method, it is recommended that more comparisons between computational results and measurements should be performed.

References

[1] Timo Siikonen, An Application of Roe's Flux-Difference Splitting for $k-\epsilon$ Turbulence Model, International Journal for Numerical Methods in Fluids, Vol. 21 No 11, p. 1017 - 1039, 1995.

[2] Siikonen, T., Hoffren, J., and Laine, S., A Multigrid LU Factorization Scheme for the Thin-Layer Navier-Stokes Equations, 17th ICAS Congress, Stockholm, 1990.

[3] IGG, Interactive Geometry Modeller and Grid Generation System, Numeca International, 1997.

[4] Uwe Seidel, Radialverdichter-Kennfeldregelung mittels Nachleitrad, Von der Fakultät für Maschinenwessen der Universität Hannover zur Erlangung des akademischen Grades Doktor-Ingenieur genehmigte Dissertation, 1995.

[5] David Japikse and Nicholas C. Baines, Introduction to Turbomachinery, ISBN 0-933283-06-7, 1994.

[6] Michael J. Moran and Howard N. Shapiro, Fundamentals of Engineering Thermodynamics, 3rd Ed., ISBN 0-471-07681-3, 1995.

8 Appendix A

8.1 Calculated results

Averaged values for p, p_0, T and T_0 have been collected for each test case in tables (7) and (8). Efficiencies have been calculated.

N_{ref}	$\dot{m_{ref}}$	p_1	T_1	p_{01}	T_{01}	p_{out}
RPM	$[kg/s]$	$[Pa]$	$[K]$	$[Pa]$	[K]	$[kPa]$
13863	3.709	126360	292.6	128257	293.9	200
13840	4.832	96397	292.6	98885	294.7	160
13952	6.571	92247	286.1	96862	285.9	140
15799	6.723	83231	291.3	87610	295.6	160
15850	7.410	74374	288.2	79227	293.6	150

Table. 7: Calculated p, T, p_0 and T_0 values for the GRV-60 impeller with the airfoil-type diffusor.

N_{ref}	$\dot{m_{ref}}$	p_1	T_1	p_{01}	T_{01}	p_{out}
RPM	$[kg/s]$	$[Pa]$	$[K]$	$[Pa]$	[K]	$[kPa]$
15819	6.125	88372	291.3	92173	294.8	170
15799	6.704	80139	291.3	84331	295.5	160

Table. 8: Calculated p, T, p_0 and T_0 values for the GRV-60 impeller with the unvaned diffusor.

8.2 Passage averaged pressures and streamlines

Figures (10), (11) and (12) show how static pressure develops in the computational domain and how the measurents agree with computational results. Streamlines on the hub and on the blade surface are shown in the Fig. (13), (14), (15), (16), (17), (18), (19), (20), (21). The difference in absolute value of momentum between the rotor and the stator is caused by different rotational co-ordinate systems.

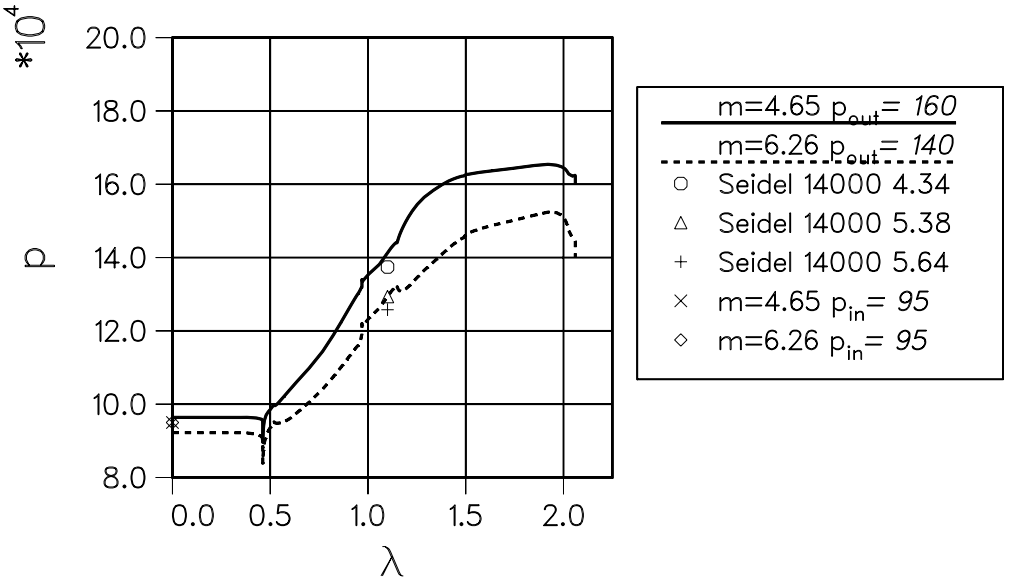

Fig. 10: Comparison of the computated mass flow averaged static pressure and the measured static pressure value at $\lambda = 1.1$ for the airfoil-type aerodynamic diffusor. The static pressure p_{in} is used to calculate the boundary values. Speed 14000 RPM.

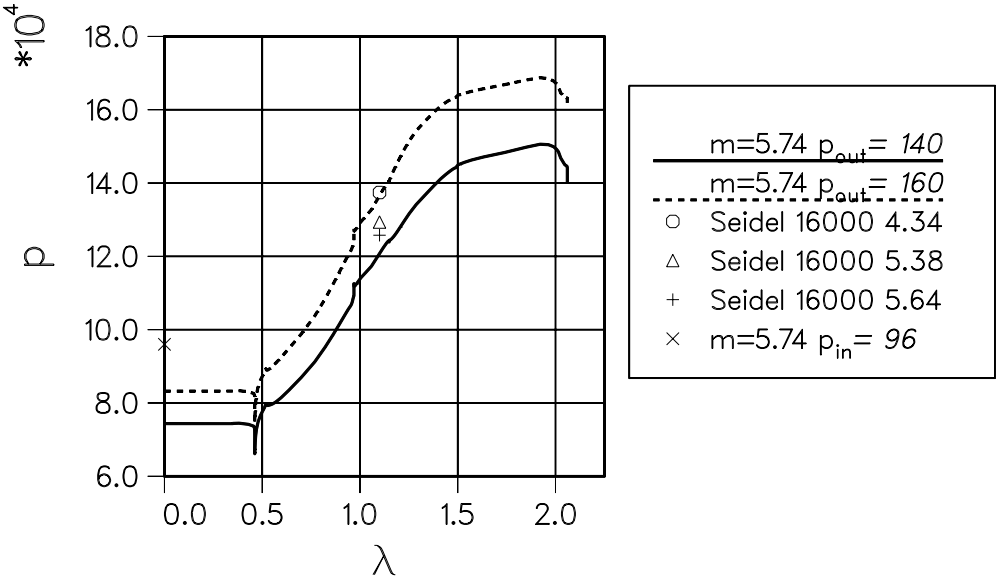

Fig. 11: Comparison of the computated mass flow averaged static pressure and the measured static pressure value at $\lambda = 1.1$ for the airfoil-type aerodynamic diffusor. Speed 16000 RPM.

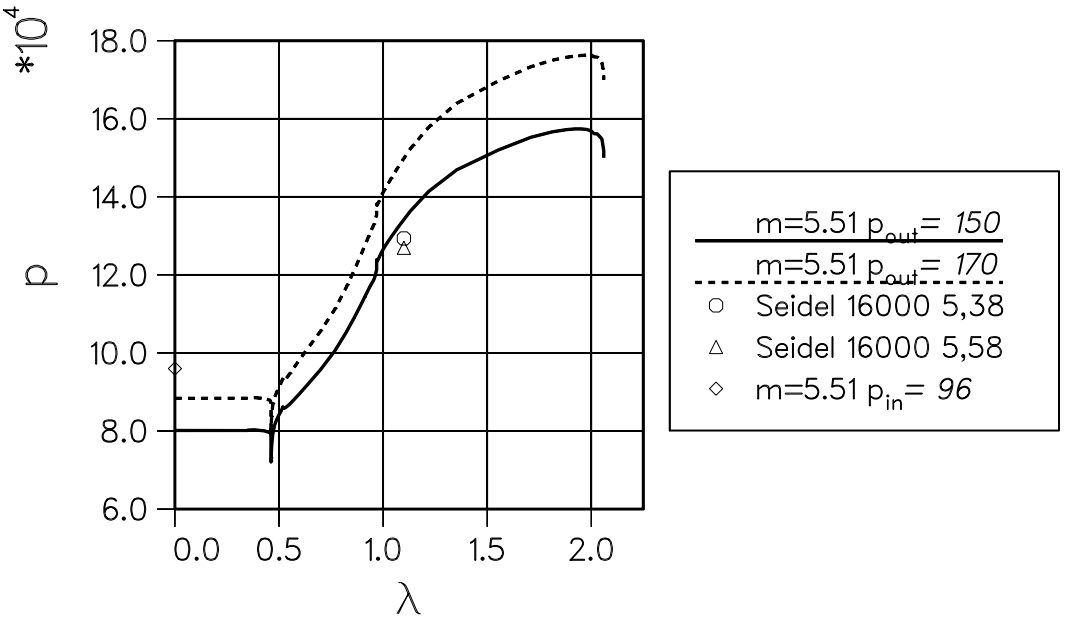

Fig. 12: Comparison of the computated mass flow averaged static pressure and the measured static pressure value at $\lambda = 1.1$ for the unvaned diffusor. Speed 16000 RPM.

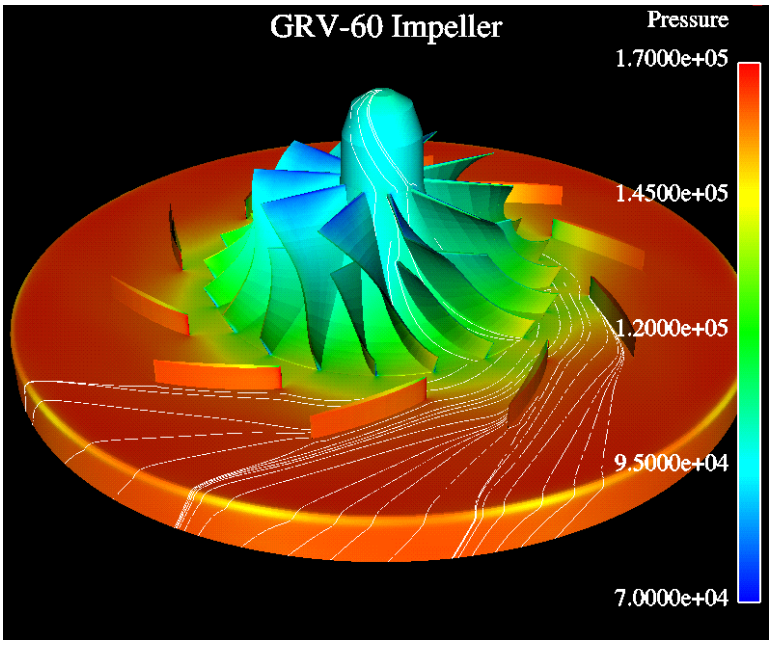

Fig. 13: The static pressure and the momentum streamlines on the surface for the airfoil-type aerodynamic diffusor. $N = 14000$ RPM, $\dot{m} = 4.65$ kg/s, $p_{out} = 160$ kPa.

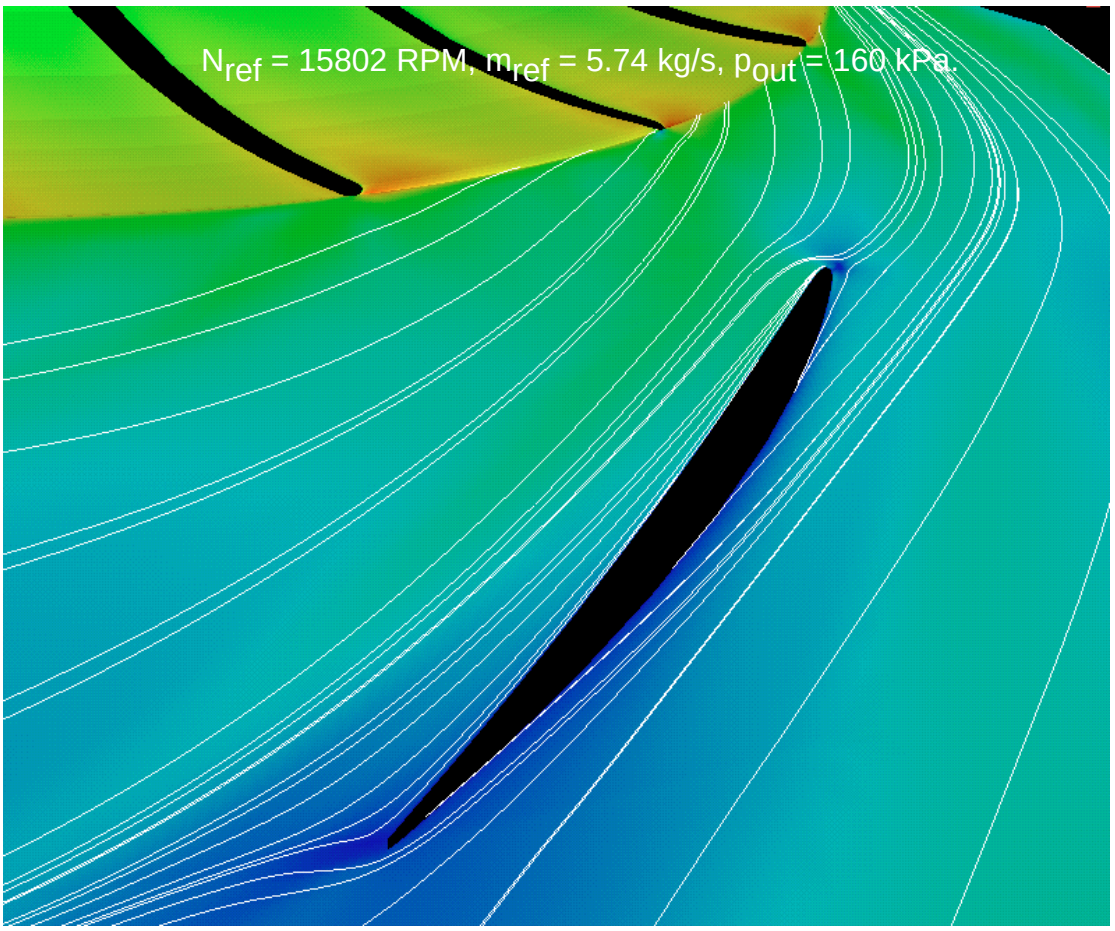

Fig. 14: Streamlines and absolute value of momentum on the grid surface J = 3 (near the hub).

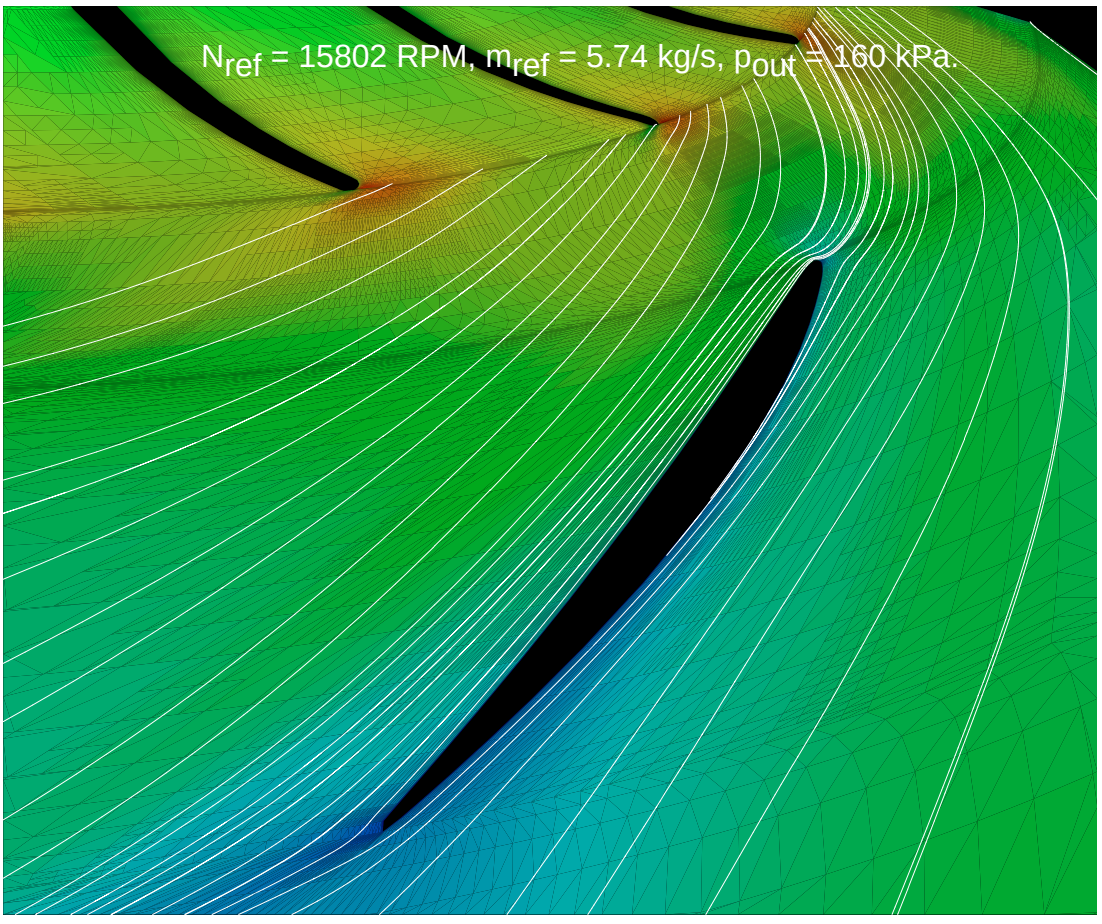

Fig. 15: Streamlines and absolute value of momentum on the grid surface J = 7 (near the hub).

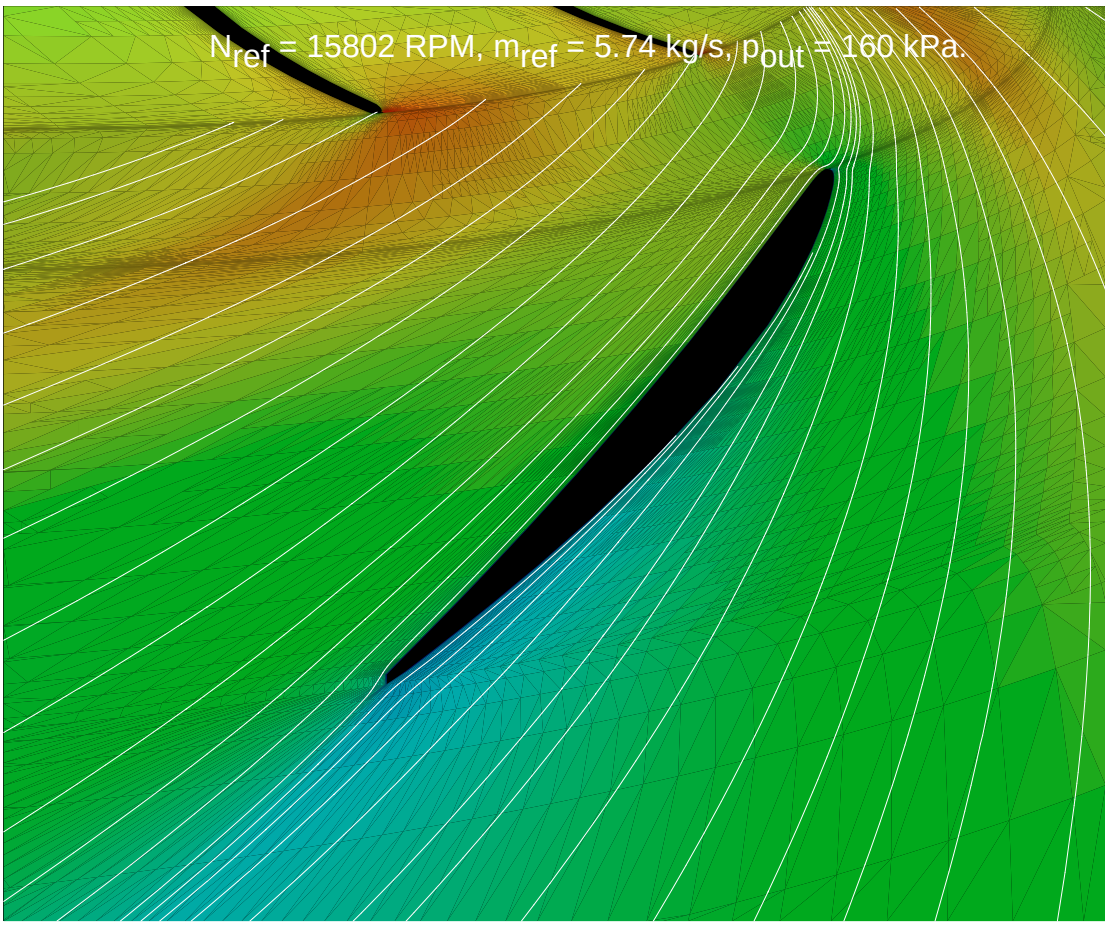

Fig. 16: Streamlines and absolute value of momentum on the grid surface J = 13 (halfway between the hub and the shroud).

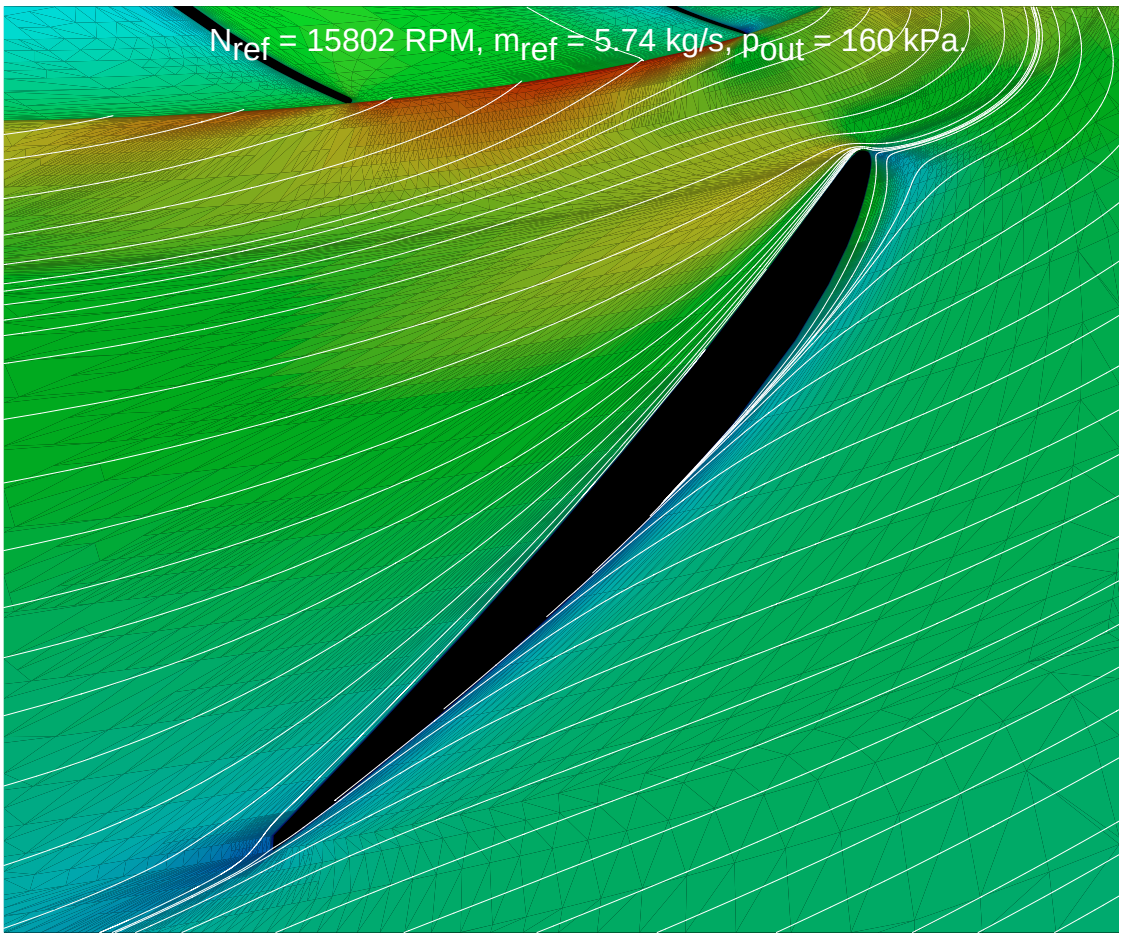

Fig. 17: Streamlines and absolute value of momentum on the grid surface J = 19 (near the shroud).

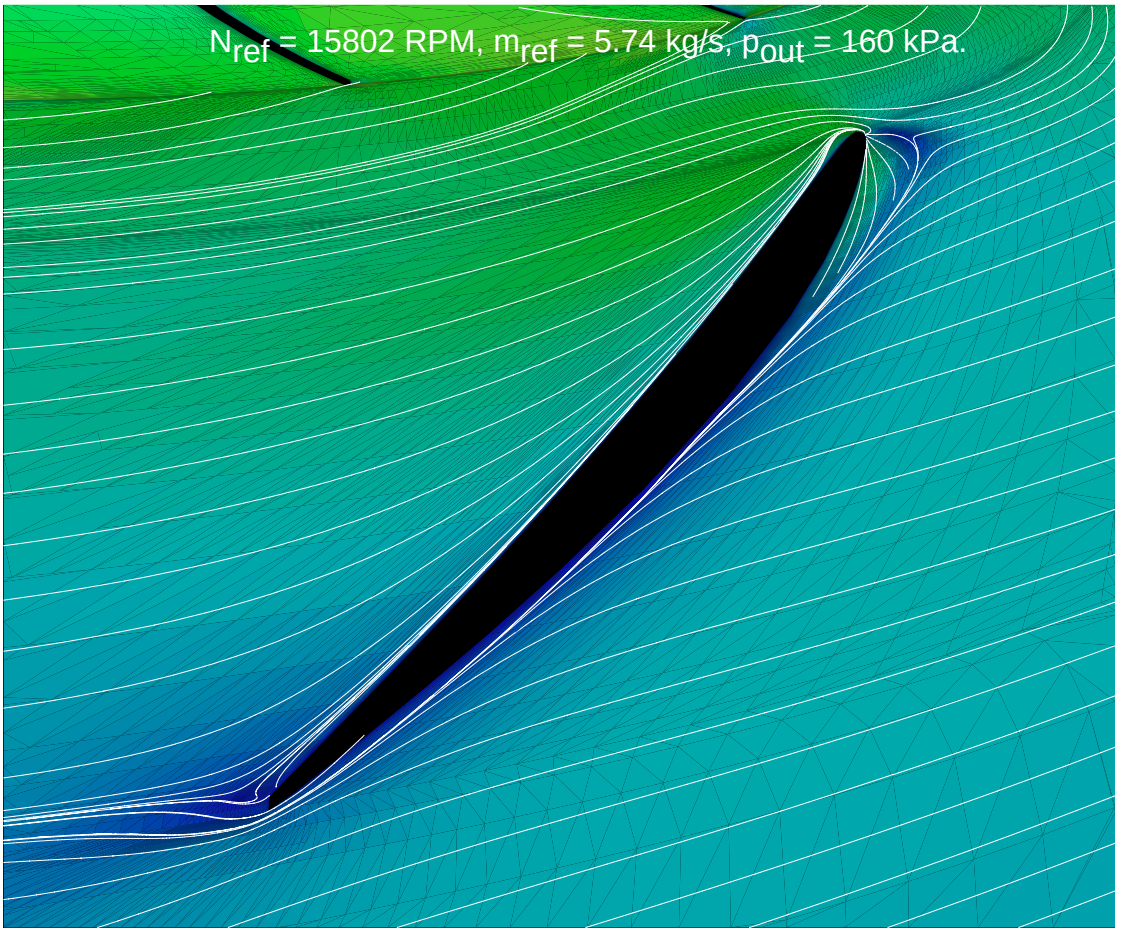

Fig. 18: Streamlines and absolute value of momentum on the grid surface J = 23 (near the shroud).

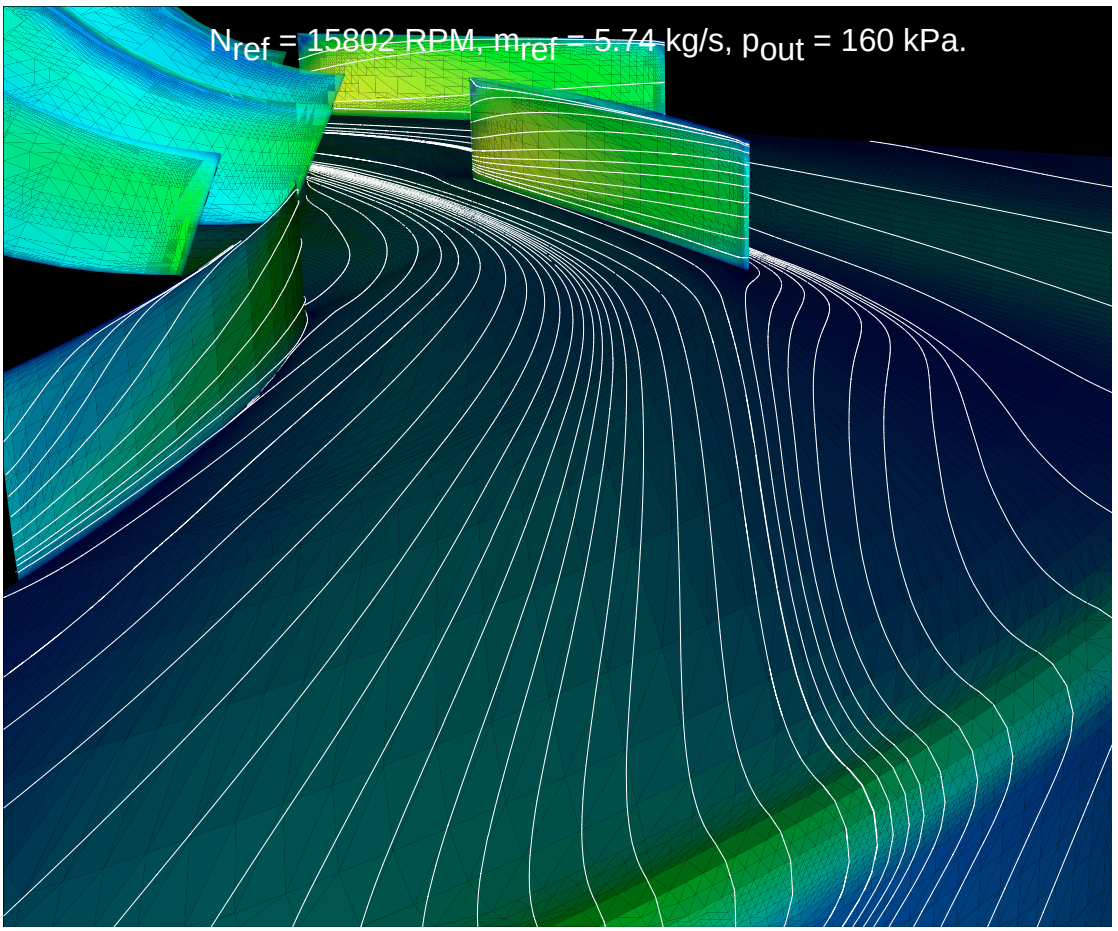

Fig. 19: Streamlines and absolute value of momentum on the grid surface J = 2 and I = 2, 64. (near the hub and the stator blade).

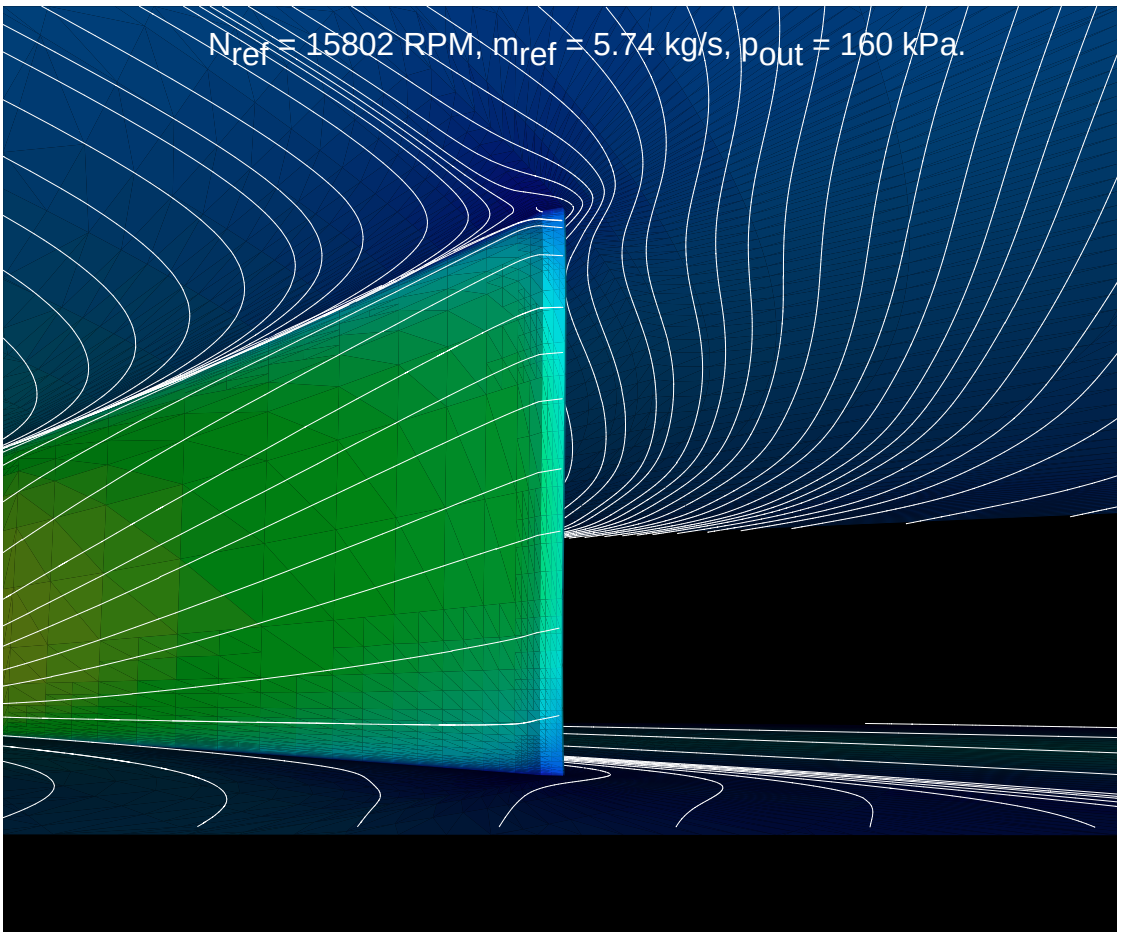

Fig. 20: A close−up view of the streamlines and absolute value of momentum on the grid surface J = 2, 24 and I = 2, 64. (near the hub, the shroud and the stator blade).

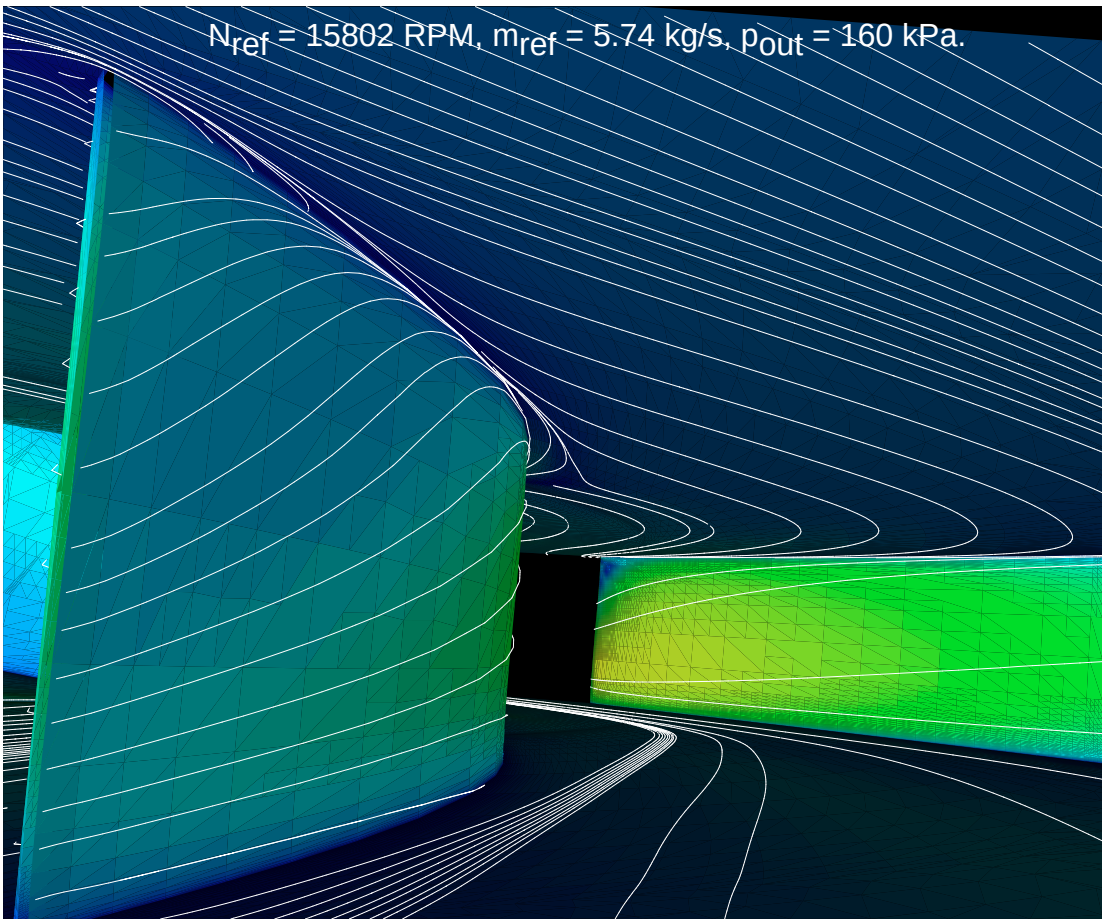

Fig. 21: A close−up view of the streamlines and absolute value of momentum on the grid surface J = 2, 24 and I = 2, 64. (near the hub, the shroud and the stator blade).